

# Helmholtz-Type Regularization Method for Permittivity Reconstruction Using Experimental Phantom Data of Electrical Capacitance Tomography

Manuchehr Soleimani, *Member, IEEE*, Phaneendra K. Yalavarthy, and Hamid Dehghani

**Abstract**—Electrical capacitance tomography (ECT) attempts to image the permittivity distribution of an object by measuring the electrical capacitance between sets of electrodes placed around its periphery. Image reconstruction in ECT is a nonlinear ill-posed inverse problem, and regularization methods are needed to stabilize this inverse problem. The reconstruction of complex shapes (sharp edges) and absolute permittivity values is a more difficult task in ECT, and the commonly used regularization methods in Tikhonov minimization are unable to solve these problems. In the standard Tikhonov regularization method, the regularization matrix has a Laplacian-type structure, which encourages smoothing reconstruction. A Helmholtz-type regularization scheme has been implemented to solve the inverse problem with complicated-shape objects and the absolute permittivity values. The Helmholtz-type regularization has a wavelike property and encourages variations of permittivity. The results from experimental data demonstrate the advantage of the Helmholtz-type regularization for recovering sharp edges over the popular Laplacian-type regularization in the framework of Tikhonov minimization. Furthermore, this paper presents examples of the reconstructed absolute value permittivity map in ECT using experimental phantom data.

**Index Terms**—Electrical capacitance tomography (ECT), forward and inverse problems, Helmholtz-type regularization, Laplacian-type regularization, permittivity imaging.

## I. INTRODUCTION

LECTRICAL capacitance tomography (ECT) seeks to image materials with a contrast in dielectric permittivity using exterior measurements of capacitance across a system of electrodes [1]–[3]. Potential applications include monitoring of oil and gas mixtures in oil pipelines and flow measurement in pneumatic conveying [4].

The inverse problem in ECT is nonlinear and ill posed, similar to the inverse conductivity problem of Calderón [9]. Regularization techniques have been adapted to stabilize the

Manuscript received July 14, 2008; revised September 1, 2008. First published August 7, 2009; current version published December 9, 2009. The Associate Editor coordinating the review process for this paper was Dr. Matteo Pastorino.

M. Soleimani is with the Department of Electronic and Electrical Engineering, University of Bath, BA2 7AY Bath, U.K. (e-mail: m.soleimani@bath.ac.uk).

P. K. Yalavarthy is with the Department of Radiation Oncology, School of Medicine, Washington University, St. Louis, MO 63110 USA.

H. Dehghani is with the School of Physics, University of Exeter, EX4 4QL Exeter, U.K.

Color versions of one or more of the figures in this paper are available online at <http://ieeexplore.ieee.org>.

Digital Object Identifier 10.1109/TIM.2009.2021645

inversion. Various image reconstruction methods have been used to solve the ECT problem, with each of them having a different regularization property. The Landweber iteration method, “linear back projection,” and a regularized one-step reconstruction method have been applied to the reconstruction of images from experimental ECT data [14], [19].

In ECT, it is highly desirable to reconstruct the absolute values of permittivity of the object. Accurate reconstruction of the permittivity values is particularly desirable in multiphase flow imaging and imaging of the concentration of the materials. Our previous study reports an improvement in the shape of reconstructed objects and the separation between nearby objects by using a nonlinear image reconstruction algorithm [3]. Based on our best knowledge, no results have been presented to show the reconstruction of the absolute permittivity values using experimental data of ECT. This paper shows the reconstruction of absolute permittivity values in two- and three-phase materials. The most common regularization in Tikhonov minimization is the standard Laplacian-type method, which is not well suited to the problems with sharp transitions in permittivity and absolute value reconstruction.

The application of total variation (TV) regularization to the general form of the elliptic inverse problem was presented in [8]. The application of TV was explored in the literature [6], [7] for electrical impedance tomography using simulated data. The application of TV regularization to reconstruct sharp edges and to account for jumps in permittivity profile using experimental data has been demonstrated in [3]. The TV regularization [10] is nonquadratic, and special attention is required to use them in a nonlinear inverse problem. In this paper, the most popular quadratic-type penalty function in the framework of Tikhonov minimization is used. Specifically, an investigation of the application of the Helmholtz-type regularization to the ECT inverse problem, along with a comparison to the commonly used Laplacian-type regularization, is presented. Therefore, the main contributions of this paper are the quantitative reconstruction of dielectric permittivity using experimental data, the use of absolute capacitance measurement data (normalized capacitance data are commonly used [2] in ECT), and a Helmholtz-type regularization method instead of the Laplacian-type regularization. These developments enabled us to reconstruct complicated-shape objects and perform quantitative permittivity reconstruction.

This paper is organized as follows. The forward and inverse ECT problems are reviewed in Section II. This includes a brief



Fig. 1. PTL ECT system showing the sensor, the ECT system, and the host computer.

discussion of the finite-element method (FEM) for modeling of the forward problem, sensitivity calculation, and nonlinear iterative methods for the inverse solution. In Section III, regularization methods for the Tikhonov minimization are explored. The main results, including the comparison of the Helmholtz-type and the Laplacian-type regularization for experimental ECT, are presented in Section IV.

## II. FORWARD PROBLEM

The computational ECT problem mainly includes the forward and inverse problems. Fig. 1 shows the eight-electrode experimental ECT system [15] that has been used for the collection of the experimental data in this paper.

The Poisson equation that is used to solve the forward problem can be given by

$$\nabla \cdot (\varepsilon \nabla u) = 0 \quad \text{in} \quad V_d \quad (1)$$

where  $u$  is the electric potential,  $\varepsilon$  is the permittivity, and  $V_d$  is the region containing the field. With a suitable boundary condition [3], [12], the forward problem can numerically be solved. Most popular numerical methods for solving the forward problem make use of FEM, as it offers flexible and reasonably accurate modelling to model the complex-shaped regions. In FEM, the imaging domain is divided into small elements (mesh) and solved assuming that the basis function that supports these elements is piecewise continuous (Galerkin formulation). Here, a 2-D FEM mesh that represents the imaging domain considered here with 6400 triangular elements was used, with the number of elements in the region of interest being 725. In the case of experimental capacitance data, the data set is commonly normalized using a calibration procedure [17]. These normalized capacitances are usually used to reconstruct ECT images [3]. Note that there is no calibration procedure involved for the experimental data used in this paper (absolute capacitance data were used in the reconstruction procedure). The sensitivity formula based on the mutual energy method [3], [5] has been used as an efficient method for calculating the updated Jacobian matrix.

## III. INVERSE PROBLEM AND REGULARIZATION METHODS

The objective function for the Tikhonov minimization method that can be used to find a distribution for  $\varepsilon$  is given by

$$\Omega = \|C_m - F(\varepsilon)\|^2 + G(\varepsilon, \varepsilon_{ref}) \quad (2)$$

where  $C_m$  is the vector of capacitance measurements, and the forward solution  $F(\varepsilon)$  is the predicted capacitance from the forward model with permittivity  $\varepsilon$ .  $G(\varepsilon, \varepsilon_{ref})$  is the penalty term (also known as the regularization term). This term is necessary to overcome the ill-posedness of the problem. Often, this incorporates the additional information about the solution space. There are different types of the regularization methods to solve an ill-posed inverse problem [21]. It is necessary for the regularization term to be complementary to the measurement data, be as realistic as possible, and more importantly be able to stabilize the inverse problem. The result of the Landweber iteration method shows an improvement in image quality compared to that of linear back projection [19]. The nonlinear Landweber iteration method will further improve the reconstructed image quality similar to other nonlinear reconstruction methods well established in ECT [3], but the number of linear iterations in each nonlinear step has to be empirically selected by the user to produce the best quality image. Other Krylov subspace methods such as preconditioned conjugate gradient [11] can also act as a regularization to constrain the solution space. The problem with this type of regularization is the difficulty associated with the inclusion of prior information. However, a thoughtful implementation can lead to a revised regularization method for improving the quality of the ECT images (discussed in [14]).

In the case of Tikhonov minimization, which is the most popular technique for solving the ill-posed problem,  $G(\varepsilon, \varepsilon_{ref})$  can be implemented in discrete form using a regularization matrix ( $L$ ), where  $\varepsilon_{ref}$  is an *a priori* guess for the permittivity distribution, and has the form of

$$G(\varepsilon, \varepsilon_{ref}) = \|\alpha(\varepsilon_n - \varepsilon_{ref})\|^2 \quad (3)$$

where  $\alpha$  is the regularization parameter that balances the data-model misfit with the penalty term. The regularization matrix  $L$  acts as a filter that can suppress the high-frequency noises. It can also include the structural prior information about the imaging domain [22], [23]. Minimizing (2) with respect to  $\varepsilon$  and linearizing the problem lead to the iterative update equation (for the  $(n+1)$ th iteration)

$$\begin{aligned} \delta\varepsilon_n = & (J_n^T J_n + \alpha^2 L^T L)^{-1} \\ & \times (J_n^T (C_m - F(\varepsilon_n)) - \alpha^2 L^T L(\varepsilon_n - \varepsilon_{ref})). \end{aligned} \quad (4)$$

In all the studies conducted here, the permittivity corresponding to free space ( $\varepsilon = 1$ ) was used as an initial guess in this iterative procedure. The Jacobian matrix  $J$  is a discretization of  $F'(\varepsilon)$ . For  $n = 1$ , this is a linear reconstruction algorithm. Here,  $J_n$  is the Jacobian calculated with permittivity  $\varepsilon_n$ . As the problem is ill posed, the condition number of  $J$  is very high. Small changes in the measurements lead to large changes in  $\varepsilon$ , making the estimation problem extremely susceptible to the system noise. To overcome this, a penalty term was added in the minimization scheme (2). Even though the penalty

term used in this paper has the form given by (3), the choice of regularization matrix  $L$  makes the type of regularization unique. The identity matrix and diagonal matrix of the so-called NOSEN Hessian regularization matrix [20] can also be used in this Tikhonov minimization scheme. The generalized singular value decomposition of the regularized system using this diagonal matrix allows the analysis of these regularization terms [21]. In this paper, a systematic comparison of the well-known Laplacian-type regularization with the Helmholtz-type regularization is presented. Sections III-A and III-B provide the details of these regularization matrices.

### A. Laplacian-Type Regularization Matrix

The Laplace equation in a variable  $\phi(x)$  is given by

$$(\nabla^2 \phi(x)) = 0. \quad (5)$$

A finite-difference method for solving the Laplace equation in one dimension having  $M$  nodes with step size  $d$  makes this equation as follows:

$$(\nabla^2 \phi(x)) d^2 = \phi_1 + \phi_2 + \cdots + \phi_{M/2} + \cdots + \phi_M = 0. \quad (6)$$

Dividing the whole domain by  $-M$  gives

$$\frac{-\phi_1}{M} + \frac{-\phi_2}{M} + \cdots + \frac{-\phi_{M/2}}{M} + \cdots + \frac{-\phi_M}{M} = 0. \quad (7)$$

This equation provides a mathematical formulation for the relation between any two points in the given region that obeys the Laplace equation. The regularization matrix  $L$  is chosen in such a way that it can relate each point in the imaging domain to the rest of the points (here, a point represents the center of each element). This leads to a matrix form of  $L$  with  $L_{ij} = 0$  if points  $i$  and  $j$  are from different regions,  $L_{ij} = -1/M$  if points  $i$  and  $j$  are in the same region ( $M$  is the number of points included in that region), and  $L_{ij} = 1$  for  $i = j$ . With this form,  $L^T L$  approximates the second-order Laplacian operator with smoothing effect for the points that belong to the same region and allows sharp transition between regions. Note that, in this paper, the whole imaging domain was chosen to be one region, making all the elements in the imaging domain connected.

### B. Helmholtz-Type Regularization Matrix

The Helmholtz equation for a damped wave in a variable  $\phi(x)$  for a wavenumber  $k$  can be written as

$$((\nabla^2 - k^2)\phi(x)) = 0. \quad (8)$$

With wavenumber  $k = 0$ , this equation becomes the Laplace equation. Similar to the finite-difference approximation to the Laplace equation, this equation can be discretized as

$$((\nabla^2 - k^2)\phi(x)) d^2 = \phi_1 + \phi_2 + \cdots + \phi_M = 0. \quad (9)$$

Dividing the equation by  $-(M + (kd)^2)$  gives

$$\begin{aligned} \frac{-\phi_1}{(M + (kd)^2)} + \frac{-\phi_2}{(M + (kd)^2)} + \cdots + \frac{-\phi_{M/2}}{(M + (kd)^2)} \\ + \cdots + \frac{-\phi_M}{(M + (kd)^2)} = 0. \end{aligned} \quad (10)$$

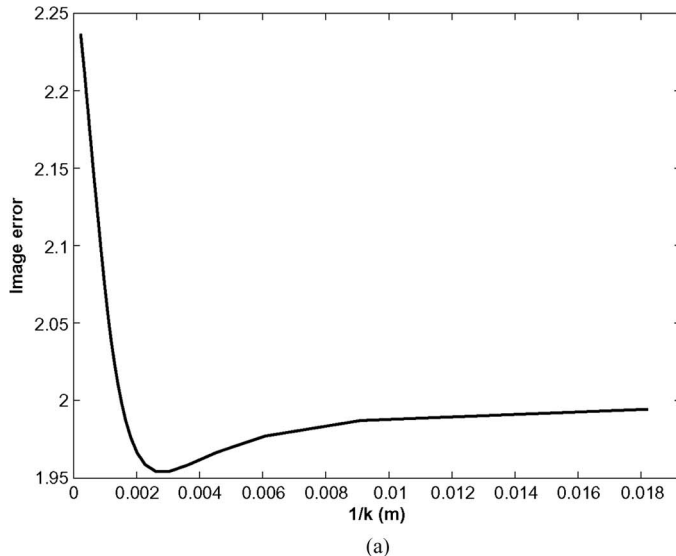
With this, an  $L$  matrix can be established that relates each point (center of an element) to all other points. Again, a region is a circle surrounding the point with a given radius (here, we choose 1/16 of the radius of the tank).  $L_{ij} = 0$  if points  $i$  and  $j$  are from different regions,  $L_{ij} = -1/(M + (kd)^2)$  if points  $i$  and  $j$  are in the same region that includes  $M$  points, and  $L_{ij} = 1$  for  $i = j$ . In this case,  $L^T L$  approximates the second-order Helmholtz equation smoothing operator. In this case,  $d$  is the distance between the points, and  $k$  is a weighting factor that can be chosen to be the inverse of the length of an inclusion based on *a priori* knowledge of the length of the inclusion.

*A priori* structural information can be included in these regularization matrices by dividing the image domain into different regions and assuming that there is no intraregion permittivity [22]. This *a priori* structural information can be developed based on a physical model such as a fluid dynamic model in multiphase flow or based on *a priori* knowledge of the internal structures for solid material inspection. Choosing  $k = 0$  converts the Helmholtz equation to the Laplace equation; furthermore, choosing the radius of the regions to be the size of the smallest element makes the regularization matrix an identity matrix.

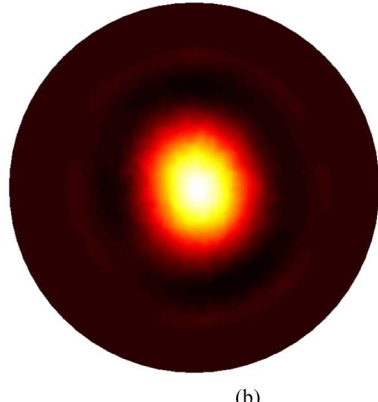
## IV. RESULTS AND DISCUSSIONS

An optimal value for  $k$  has been selected based on the smallest error between observed and reconstructed values. To evaluate the performance of the Helmholtz-type and the Laplacian-type regularization method, ECT measurement data were collected with various object shapes. The shape of the objects was chosen to represent the sharp transition in permittivity profile. The objects were cross-shaped, "T"-shaped, "V"-shaped, and rectangular-shaped objects. The absolute values of the permittivity distributions and visual inspection of the images are used to evaluate the performance of the regularization methods. The circular region of interest for imaging has a diameter of 150 mm. In all experimental test examples, six iterations of a Gauss-Newton algorithm are used to solve the nonlinear image reconstruction (with recalculation of the Jacobian at each iteration) problem of ECT [3]. To compare the performance of the Helmholtz-type with the Laplacian-type regularization, the regularization parameter  $\alpha = \alpha_1 \times \|J\|/\|L\|$  (where  $J$  is the first Jacobian) was selected so that the two methods can be compared with the same amount of regularization for a given  $\alpha_1$ .

In the simulated ECT data in Fig. 2, a circular inclusion of radius 20 mm from the center with a relative permittivity of 1.8 and  $\alpha_1 = 10^{-4}$  was chosen, and the variable  $k$  was changed, with an image error of  $\|\varepsilon_6 - \varepsilon_{\text{true}}\|$ , where  $\varepsilon_6$  is the reconstructed permittivity of the sixth iteration of nonlinear inverse solver, and  $\varepsilon_{\text{true}}$  is the true permittivity distribution. Fig. 2(a) shows that  $1/k = 0.003$  m provides an optimal value to generate the best image, which is shown in Fig. 2(b). In this example, a noise with a standard deviation of 0.5% was added to the simulated data. The optimal  $k$  value obtained from the aforementioned example was used in the following experimental data cases.



(a)

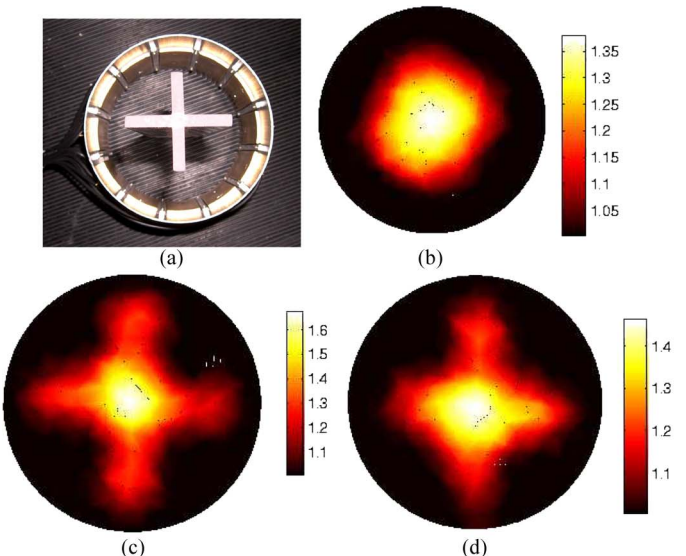


(b)

Fig. 2. (a) Effect of  $k$  in the reconstructed image. (b) Reconstructed image with  $1/k = .003$ .

Fig. 3 shows the reconstructed images of a plastic object (with a permittivity of 1.7) with a cross shape using experimental (phantom) data. The Helmholtz-type regularization and the Laplacian-type regularization were used to reconstruct these images. Different values of the regularization parameters are used to study the effect of the amount of regularization. With the regularization parameter  $\alpha_1 = 10^{-2}$ , which represents a higher level of regularization (more emphasis on the penalty term), the Helmholtz-type reconstruction shows the cross shape, and the Laplacian-type regularization tends to smooth out the object. Fig. 3(f) shows a reduction in mismatch error (norm of differences) between measured and simulated capacitance data with the iteration of the nonlinear inverse solver. Similar results were found using “T”-shaped objects and various “V”-shaped objects, where the Helmholtz-type method outperforms the Laplacian-type method. Fig. 4 shows the reconstruction of a “V”-shaped object using the Helmholtz-type and the Laplacian-type regularization method.

Fig. 5 shows another challenging example, i.e., that of two rectangular wooden objects. Various regularization values were tested, and the best images could be reconstructed using the Helmholtz-type regularization. The absolute value of permittivity could satisfactorily be reconstructed after nonlinear it-



(a)

(b)

(c)

(d)

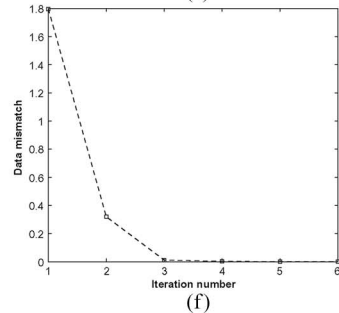


Fig. 3. Reconstruction of a cross-shaped plastic object from experimental data using Helmholtz and Laplacian regularization. The experimental data were collected by PTL. (a) A cross-shape inclusion. (b) Laplacian reconstruction with regularization parameter  $10^{-2}$ . (c) Helmholtz reconstruction with regularization parameter  $10^{-2}$ . (d) Laplacian reconstruction with regularization parameter  $10^{-4}$ . (e) Helmholtz reconstruction with regularization parameter  $10^{-4}$ . (f) Reduction in mismatch error between simulated and measured data by nonlinear iteration for (e).

erations, particularly when the Helmholtz-type regularization is used.

Fig. 6 shows a successful reconstruction of three different permittivity materials. A rectangular-shaped wooden object and a circular-shaped plastic object are reconstructed in an air background. The resulting reconstruction images show better corner detection in the rectangular-shaped object and better quantification of permittivity values using the Helmholtz-type regularization. It can also be seen that the Laplacian-type regularization produces a smoother image with fewer artifacts than the Helmholtz regularization. In this paper, we did not find a systematic way to find the optimal value of  $k$ . All simulation results, same as Fig. 2, shows that the optimal  $k$  is not  $k = 0$ , which is the commonly used Laplacian method; a selection

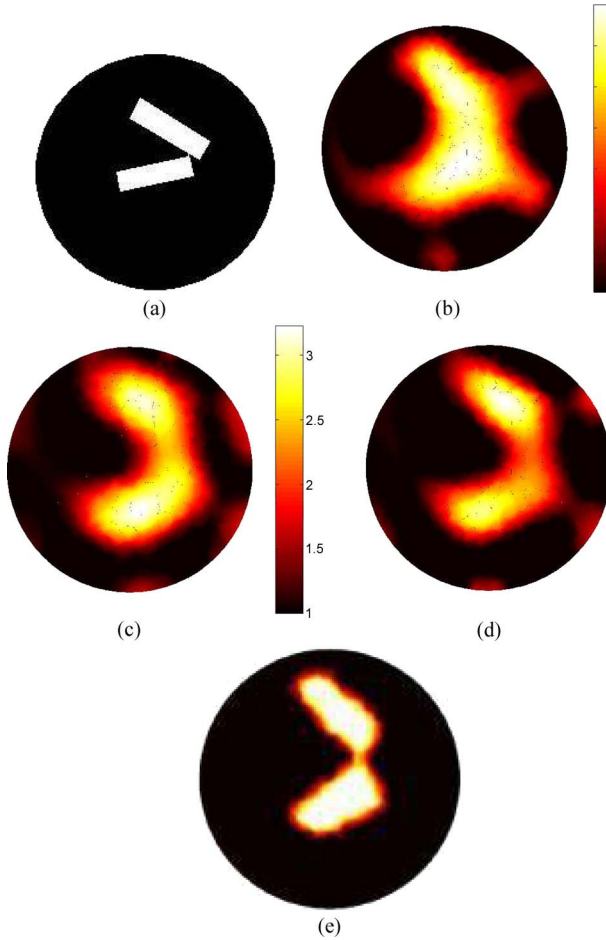


Fig. 4. Reconstruction of a V-shaped wooden object from experimental data using Helmholtz regularization. The experimental data were collected by PTL. (a) V-shaped object. (b) Tikhonov reconstruction with regularization parameter  $10^{-4}$ . (c) Helmholtz reconstruction with regularization parameter  $10^{-4}$ , using normalized capacitance data, where the higher permittivity filling was plastic with permittivity of 1.7. (d) Helmholtz reconstruction with regularization parameter  $10^{-4}$ . (e) Helmholtz image with upper and lower permittivity thresholds of 1 and 2.1, respectively.

of  $k$  that creates a wavenumber that is the same size as the smallest object (smaller corner of a complex object) is a suitable choice. More studies are needed for the optimal selection of the  $k$  parameter.

## V. CONCLUSION

A linear iteration scheme such as the Landweber iteration method can act as a regularization tool, but it is difficult to include prior information in the reconstruction scheme. Here, a simple framework that can utilize the prior information in the regularization matrices, which have the equivalent forms of Laplacian and Helmholtz, has been presented. The Laplacian-type regularization assumes the smoothness of the permittivity distribution, so the sharp edges cannot easily be recovered. However, the shape of the targets can more accurately be detected by using the Helmholtz-type regularization, which encourages the spatial correlation of permittivity variation. The Helmholtz-type regularization can be seen as a more generalized method for incorporating the structure *a priori* in image reconstruction of ECT.

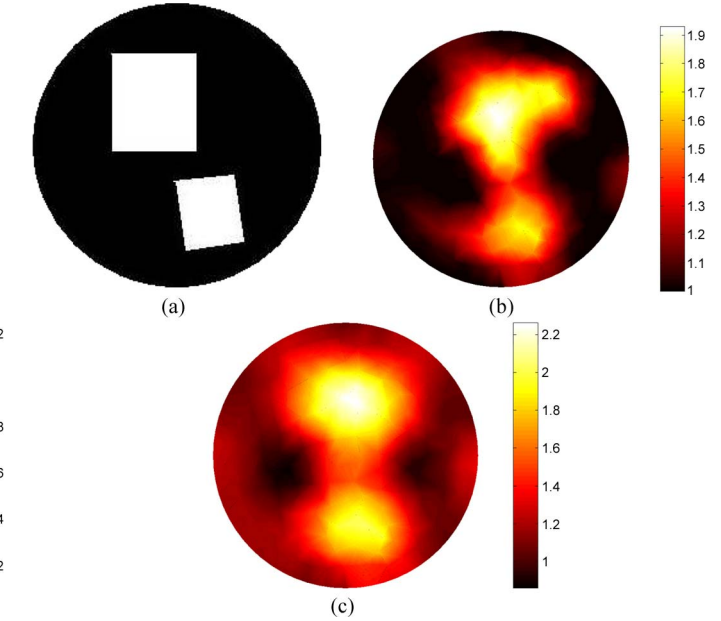


Fig. 5. Reconstruction of two rectangular-shaped wooden objects from experimental data using Helmholtz-type and Laplace regularization. The experimental data were collected by PTL. (a) True shape. (b) Laplace reconstruction with regularization parameter  $10^{-4}$ . (c) Helmholtz-type reconstruction with regularization parameter  $10^{-4}$ .

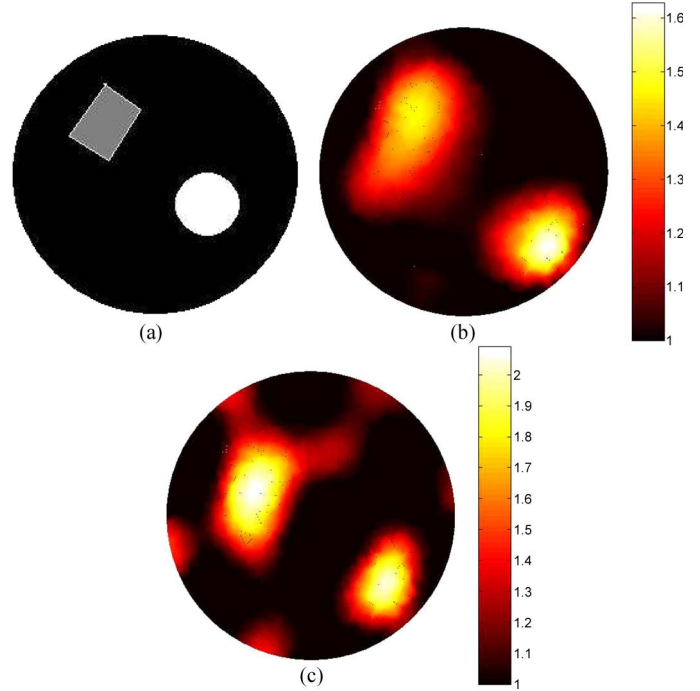


Fig. 6. Reconstruction of a rectangular-shaped wooden object and a circular plastic object from experimental data using Helmholtz-type and Laplacian-type regularization. The experimental data were collected by PTL. (a) True shape. (b) Laplacian reconstruction with regularization parameter  $10^{-4}$ . (c) Helmholtz-type reconstruction with regularization parameter  $10^{-4}$ .

The Helmholtz-type regularization matrix implemented in this paper has some measure of difference between neighboring pixels weighted by the distance between two pixels. The measure of differences between pixel values can help to recover the permittivity jumps and consequently achieve better absolute value and edge detection.

This paper has compared the Helmholtz-type and Laplacian-type regularization methods for challenging inverse problems that uses ECT experimental (phantom) data. The Helmholtz-type regularization is more reliable in recovering the shape function compared to the Laplacian-type regularization with the same level of regularization. The absolute permittivity values reconstructed in this paper are the first absolute permittivity reconstruction using ECT experimental data and without additional constraints. The absolute value reconstruction using the Helmholtz-type regularization shows better agreement with the actual permittivity of the object.

## REFERENCES

- [1] O. Isaksen, "A review of reconstruction techniques for capacitance tomography," *Meas. Sci. Technol.*, vol. 7, no. 3, pp. 325–337, Mar. 1996.
- [2] W. Q. Yang and L. H. Peng, "Image reconstruction algorithms for electrical capacitance tomography," *Meas. Sci. Technol.*, vol. 14, no. 1, pp. R1–R13, Jan. 2003.
- [3] M. Soleimani and W. R. B. Lionheart, "Nonlinear image reconstruction in electrical capacitance tomography using experimental data," *Meas. Sci. Technol.*, vol. 16, no. 10, pp. 1987–1996, Oct. 2005.
- [4] T. Dyakowski, L. F. C. Jeanmeure, W. B. Zimmerman, and W. Clark, "Direct flow-pattern identification using electrical capacitance tomography," *Exp. Therm. Fluid Sci.*, vol. 26, no. 6/7, pp. 763–773, Aug. 2002.
- [5] B. Brandstätter, G. Holler, and D. Watzenig, "Reconstruction of inhomogeneities in fluids by means of capacitance tomography," *COMPEL-Int. J. Comput. Math. Elect. Electron. Eng.*, vol. 22, no. 3, pp. 508–519, 2003.
- [6] A. Borsic, C. N. McLeod, and W. R. B. Lionheart, "Total variation regularisation in EIT reconstruction," in *2nd World Congr. Ind. Process Tomography*, Hannover, Germany, 2001, pp. 579–587.
- [7] A. Borsic, W. R. B. Lionheart, and C. N. McLeod, "Generation of anisotropic-smoothness regularization filters for EIT," *IEEE Trans. Med. Imag.*, vol. 21, no. 6, pp. 576–587, Jun. 2002.
- [8] T. F. Chan and X. C. Tai, "Level set and total variation regularization for elliptic inverse problems with discontinuous coefficients," *J. Comput. Phys.*, vol. 193, no. 1, pp. 40–66, Jan. 2004.
- [9] A. P. Calderón, "On an inverse boundary value problem," in *Seminar on Numerical Analysis and Its Applications to Continuum Physics*. Rio de Janeiro, Brazil: Soc. Brasil. Mat., 1980, pp. 65–73.
- [10] C. R. Vogel, *Computational Methods for Inverse Problems*, ser. Frontiers in Applied Mathematics. Philadelphia, PA: SIAM, 2002.
- [11] N. Polydorides, W. R. B. Lionheart, and H. McCann, "Krylov subspace iterative techniques: On the detection of brain activity with EIT," *IEEE Trans. Med. Imag.*, vol. 21, no. 6, pp. 596–603, Jun. 2002.
- [12] S. Gomez, O. Michiyo, C. Gamio, and A. Fraguela, "Reconstruction of capacitance tomography images of simulated two-phase flow regimes," *Appl. Numer. Math.*, vol. 46, no. 2, pp. 197–208, Aug. 2003.
- [13] G. Holler, D. Watzenig, and B. Brandstätter, "A fast Gauss-Newton based ECT algorithm with automatic adjustment of the regularization parameter," in *Proc. 3rd World Congr. Ind. Process Tomography*, Banff, AB, Canada, 2003, pp. 415–420.
- [14] J. Zhao, W. Fu, T. Li, and S. Wang, "An image reconstruction algorithm based on a revised regularization method for electrical capacitance tomography," *Meas. Sci. Technol.*, vol. 13, no. 4, pp. 638–640, Apr. 2002.
- [15] PTL. [Online]. Available: <http://www.tomography.com>
- [16] W. Warsito and L. S. Fan, "Neural network based multi-criterion optimization image reconstruction technique for imaging two- and three-phase flow systems using electrical capacitance tomography," *Meas. Sci. Technol.*, vol. 12, no. 12, pp. 2198–2210, Dec. 2001.
- [17] W. Q. Yang, "Calibration of capacitance tomography systems: A new method for setting system measurement range," *Meas. Sci. Technol.*, vol. 7, no. 6, pp. L863–L867, Jun. 1996.
- [18] W. Q. Yang, D. M. Spink, T. A. York, and H. McCann, "An image-reconstruction algorithm based on Landweber's iteration method for electrical-capacitance tomography," *Meas. Sci. Technol.*, vol. 10, no. 11, pp. 1065–1069, Nov. 1999.
- [19] J. Locker and P. M. Prenter, "Regularization with differential operators. I. General theory," *J. Math. Anal. Appl.*, vol. 74, no. 2, pp. 504–529, Apr. 1980.
- [20] M. Cheney, D. Isaacson, J. C. Newell, S. Simske, and J. Goble, "NOSER: An algorithm for solving the inverse conductivity problem," *Int. J. Imaging Syst. Technol.*, vol. 2, no. 2, pp. 66–75, 1990.
- [21] P. C. Hansen, *Rank-Deficient and Discrete Ill-Posed Inverse Problems*. Philadelphia, PA: SIAM, 1998.
- [22] P. K. Yalavarthy, B. W. Pogue, H. Dehghani, C. M. Carpenter, S. Jiang, and K. D. Paulsen, "Structural information within regularization matrices improves near infrared diffuse optical tomography," *Opt. Express*, vol. 15, no. 13, pp. 8043–8058, Jun. 2007.
- [23] P. K. Yalavarthy, B. W. Pogue, H. Dehghani, and K. D. Paulsen, "Weight-matrix structured regularization provides optimal generalized least-squares estimate in diffuse optical tomography," *Med. Phys.*, vol. 34, no. 6, pp. 2085–2098, Jun. 2007.



**Manuchehr Soleimani** (M'06) received the B.Sc. degree in electrical engineering and the M.Sc. degree in biomedical engineering from the Sharif University of Technology, Tehran, Iran, in 1996 and 1999, respectively, and the Ph.D. degree in inverse problems and electromagnetic tomography from the University of Manchester, Manchester, U.K., in 2005.

From 2005 to 2007, he was a Research Associate with the School of Materials, University of Manchester, where he developed a range of wearable devices and biomedical textile. In 2007, he joined the Department of Electronic and Electrical Engineering, University of Bath, Bath, U.K., where he was first a Research Associate and then became a Lecturer in 2008. He is the author of more than 120 journal papers, review papers, book chapters, and papers in conference proceedings. He is the holder of several patents. He has edited three special issues in journals and is serving as an editorial board member of four scientific journals.



**Phaneendra K. Yalavarthy** received the B.Sc. and M.Sc. degrees in physics from Sri Sathya Sai University, Prasanthi Nilayam, India, in 1999 and 2001, respectively, the M.Sc. degree in engineering from the Indian Institute of Science, Bangalore, India, in 2004, and the Ph.D. degree in biomedical computation, working as a U.S. Department of Defense Breast Cancer Predoctoral Fellow, from Dartmouth College, Hanover, NH, in 2007.

He is currently a Postdoctoral Research Associate with the Department of Radiation Oncology, School of Medicine, Washington University, St. Louis, MO. His research interests include computational methods in medical imaging and radiation therapy, inverse problems in medical imaging, breathing motion modeling, 4-D computed tomography, and 4-D positron emission tomography.

Dr. Yalavarthy is a member of American Association of Physicists in Medicine.



**Hamid Dehghani** received the B.Sc. degree in biomedical and bioelectronic engineering from the University of Salford, Salford, U.K., in 1994 and the M.Sc. degree in medical physics and clinical engineering and the Ph.D. degree in medical imaging in 1999 from Sheffield Hallam University, Sheffield, U.K.

For three years, he was a Research Assistant with University College London, London, investigating near-infrared imaging of the neonatal brain. From 2001 to 2005, he was an Assistant Professor of engineering with the Thayer School of Engineering, Dartmouth College, Hanover, NH. He is currently a Lecturer with the School of Physics, University of Exeter, Exeter, U.K. His research interests include numerical modeling and image reconstruction for both electrical impedance and optical tomography.